ChemPubSoc Europe
DOI: 10.1002/chem.201600670
CHEMISTRY
A European Journal
Full Paper

Ionic Liquids

Insights into the Formation and Structures of Molecular Gels by Diimidazolium Salt Gelators in Ionic Liquids or “Normal” Solvents

Carla Rizzo,[a] Francesca D’Anna,*[a] Renato Noto,[a] Mohan Zhang,[b] and Richard G. Weiss[b, c]

Abstract: Insights are provided into the properties of molecular gels formed by diimidazolium salts both in “normal” solvents and ionic liquids. These materials can be interesting for applications in green and sustainable chemistry in which ionic liquids play a significant role, like catalysis and energy. In particular, two positional isomers of a diimidazolium cation have been examined with a wide range of anions for their ability to form gel phases. In particular, di-, tri-, and tetravalent anions bearing aliphatic or aromatic spacers were paired with the divalent cations. The properties of the organo- and ionogels formed have been analyzed by means of several different techniques, including calorimetry, rheology, resonance light scattering, UV/Vis absorption, polarizing optical microscopy, and powder X-ray diffraction measurements. The investigations performed enabled us to obtain a wide range of conductive materials characterized by a high thermal stability and a low corrosiveness of the gelator (organogels) or of both gelator and solvent (ionogels). The information gained should be useful in the broader quest to identify and promote their applications.

Introduction

The search for new materials that could be applied in green and sustainable chemistry area is one of the main goals of current chemistry research. In particular, important fields like catalysis and energy are continuously demanding new systems, more stable and easier to handle than the liquid ones so far developed. Gel phases, and supramolecular gels in particularly seem good candidates to this aim. They are formed by low molecular weight gelators (LMWGs) that possess the ability to immobilize solvents by forming a 3-dimensional (3D) network.[1] However, the processes by which self-assembly occurs are very complex.[2] In fact, the majority of supramolecular gel types has been discovered serendipitously, even though some research groups have employed comprehensive approaches that include experimental and computational methods in an attempt to devise a priori recipes for the design of gelators and self-assembled fibrillar networks (SAFINs).[3]

Supramolecular gels combine the ordered structure and confined environment of solids with the properties of liquids and this should represent a significant advantage from the catalysis point of view. However, despite the above-mentioned advantages, possible solvent volatility and matrix damages during the process still remain serious issues, whenever organo- or hydrogels are concerned.

On the other hand, as far as applications in energy are considered, satisfactory conductivity is a requested feature. Again the nature of the electrolyte and the solvent volatility are the main current limitations. Organic salts and ionic liquids (ILs) may represent a good combination in attempt to solve all the above-mentioned problems. In this regard, organic salts have recently gained the attention of researchers as LMWGs to form supramolecular gels. Indeed, many salts can be easily synthesized, and small modifications of their structures can result in formation of materials with very different properties.[4] In addition, organic salts are less corrosive than inorganic molten salts, which represents a significant advantage whenever applications of the corresponding gel materials, such as dye-sensitized solar cells (DSSCs), electrocatalysis/supercapacitors and fuel cells are taken into account.

On the other hand, since their first appearance in literature, ILs have been widely used both in catalysis and energy production and storage.[5] Self-assembly with ILs leads to the formation of ionogels that are soft materials having both high thermal stability and conductivity.[6] These properties, in addition to low vapor pressures and low flammability, are found in the ILs alone.[7] In particular, most of typical IL properties, such as conductivity, are not diminished in the ionogels; in some cases, they are even enhanced. The beneficial ability to immobilize ILs in a SAFIN opens several possibilities for new applications.[8] For instance, the use of ionogels in DSSCs avoids leakage problems, which occur when ILs are used alone.[9]

---

[a] Dr. C. Rizzo, Prof. F. D’Anna, Prof. R. Noto
Università degli Studi di Palermo, Dipartimento STEBICEF
Sezione di Chimica, Viale delle Scienze, Parco O’Orleans II
90128 Palermo (Italy)
E-mail: francesca.danna@unipa.it

[b] M. Zhang, Prof. R. G. Weiss
Department of Chemistry, Georgetown University
Washington, DC, 20057-1227 (USA)

[c] Prof. R. G. Weiss
Institute for Soft Matter Synthesis and Metrology, Georgetown University
Washington, DC, 20057-1227 (USA)

Supporting information and the ORCID identification number(s) for the author(s) of this article can be found under http://dx.doi.org/10.1002/chem.201600670.

Kimizuka first defined "ionogels" referring to polymers able to aggregate IL solutions.[10] Nowadays, this term comprises a wide variety of materials, including polymeric gels, hydride materials containing inorganic species, and recently supramolecular gels too.[11]

Literature on gels formed by ILs has been recently reviewed by Marr et al.[12] However, few examples have been reported so far regarding the gelation of organic salts or ILs in IL solution. In the latter case, of course the domains formed are characterized by the presence of one IL acting as the liquid phase and the other one as the solid continuous phase. The materials obtained should be able to fulfill the requests of green and sustainable chemistry.

In particular, Hao et al. reported the formation of an anisotropic, thermally-reversible ionogel with sodium laurate as the LMWG.[13] Zhou et al. developed an anticorrosive/antioxidant supramolecular gel, in which the LMWG is an imidazolium-type "ionic liquid" bearing a benzotriazole group.[14] Furthermore, Yan et al. have made new conductive materials for DSSCs that involve ionogel formation by host–guest interactions between organic salts and β-cyclodextrins.[15] In the framework of our interest in studying properties and applications of organic salts,[16] we recently obtained supramolecular gels in IL solution from dicationic organic salts that exhibit a high structural order degree. The materials obtained showed similar or higher conductivities as compared to neat ILs.[17] Obviously, the large number of cation/anion combination claimed for ionic liquids can be also reasserted for organic salts. Consequently, gelation of organic salts in ILs can give a huge number of soft materials having significantly different properties. This brings about the need to have a deep knowledge of the properties of ionogel phases to better identify their practical potentialities.

In the present work, we study the properties and the gelating abilities of two isomeric diimidazolium organic cations, namely 3,3′-di-*n*-dodecyl-1,1′-(1,4-phenylenedimethylene)diimidazolium (*p*-C_{12}im) and 3,3′-di-*n*-dodecyl-1,1′-(1,3-phenylenedimethylene)diimidazolium (*m*-C_{12}im) in which the counterions are aliphatic or aromatic carboxylate anions that differ in the extension of their π-surfaces and the number of negative charges (2,6-naphtalenedicarboxylate (2,6-NDC), 1,4-benzenedicarboxylate (1,4-BDC), trimesate (Trim), citrate (Cit), ethylendiaminetetracetate (EDTA)) (Scheme 1). Previously, we demonstrated by DFT calculations that the substitution pattern of the dications is a key factor in determining the efficiency of the gelation process due to the different packing modes that the *meta* and *para* isomers require, especially when paired with their anions.[18] In this work, we analyze how the combination of these two dications with di-, tri-, or tetra anions influences the gelating ability of the organic salts with several ILs and with conventional solvents. Indeed, the different stoichiometries between the dications and their anions (1:1, 3:2, or 2:1) can lead to different packing arrangements of the salts. Different stoichiometric dication to anion ratios in the salt composition were expected to have important consequences on the favorability of interactions leading to gel formation.

Among the ILs, imidazolium ILs having anions that differ in size, symmetry, and coordinating ability ([bmim][BF_4], [bmim][PF_6], [bmim][SbF_6], [bmim][NTf_2]), and a pyrrolidinum IL ([bmpyrr][NTf_2]) have been examined as gelation solvents (Scheme 1). Specifically, the thermal properties of the neat organic salts have been investigated using thermogravimetric (TGA) and differential scanning calorimetry (DSC) analyses. The thermal stabilities of the gels have been investigated using the falling-ball method[19] and DSC measurements, whereas their mechanical and thixotropic properties were examined by rheology. Furthermore, the ability of the gels to self-repair was analyzed by subjecting them to ultrasound and magnetic stirring. Finally, the gelation processes have been investigated by resonance light scattering (RLS) and UV/Vis and rheology measurements, and the morphologies of the SAFINs have

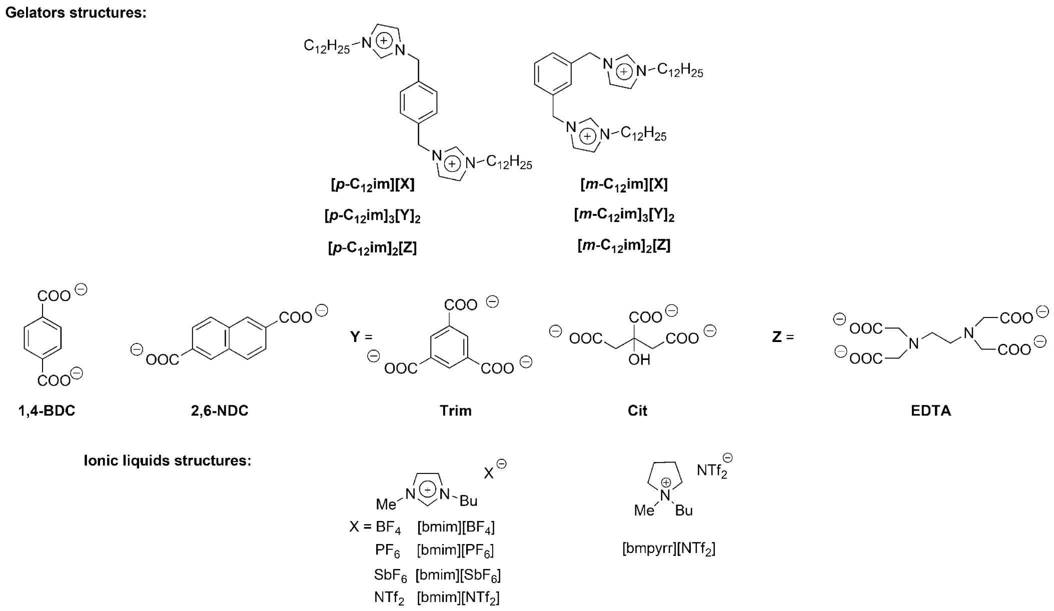

Scheme 1. Structures of diimidazolium salts used as gelators and ionic liquids used as the solvent components.

been studied by polarizing optical microscopy (POM) and powder X-ray diffraction (PXRD).

Results and Discussion

Thermal analysis of organic salts

Before testing the gelating abilities of the salts, their thermal stabilities were evaluated by TGA and DSC measurements (the Supporting Information, Figures S1, S2 and Table S1). In particular, the decomposition temperatures (T_d), melting temperatures (T_m), variations of enthalpy corresponding to the melting processes (ΔH_m), and of glass transition temperatures (T_g) were determined at the maximum slopes of TGA derivative curves, as the maximum of heat flows in the DSC thermograms, as the integrated areas of the melting calorimetric peaks, and as the onset points of the sigmoidal curves of heat flow in the DSC thermograms, respectively.

In all cases, a single-step decomposition process was observed and T_d ranges were from 206 °C for [p-C_{12}im]$_3$[Cit]$_2$ to 245 °C for [m-C_{12}im][2,6-NDC]. Although the thermal stability of these organic salts is high, it is lower than those reported by Armstrong et al. for some diimidazolium salts bearing aliphatic spacers.[20]

Perusal of the data in Table S1 indicates that the thermal properties are affected significantly by the nature of both the isomeric cation and the anions. In general, *para* isomers show lower T_d values than those of the corresponding *meta* isomers. T_d decreases on going from bivalent to trivalent anions and, in the latter case, it decreases on going from aromatic to aliphatic ones ([Trim] > [Cit]). However, for aliphatic anions, [EDTA] stabilizes better the salts. Furthermore, in agreement with thermal stability of some dioctylimidazolium salts,[21] the increase in π-surface area of aromatic dianions increased T_d, as evidenced from the comparison between [m-C_{12}im][1,4-BDC] and [m-C_{12}im][2,6-NDC].

Also, DSC thermograms revealed polymorphism in the compounds.[22] Indeed, more than one endotherm can be detected during the first heating. The second and third heating cycles are reproducible and indicate the stability of the salts. This behavior appears to depend on the solvent of crystallization and on the time needed for a salt to return to its initial morph (if it is more stable thermodynamically than the one from solidification of the melt; see below). In some cases, the first heating thermograms revealed a small and second endotherm. However, no evidence for mesophases was found using polarized optical microscopy. Consequently, we ascribe these transitions to melting processes. With the exception of the DSC thermograms of [p-C_{12}im][2,6-NDC], [p-C_{12}im]$_2$[EDTA] and [m-C_{12}im]$_2$[EDTA], the second and third heating thermograms showed only glass transitions.

In agreement with what is known about salts with similar structures,[18,23] the higher T_m and T_g values of [p-C_{12}im] isomers than those of the corresponding [m-C_{12}im] isomers are consistent with the latter having lower structural order. However, there is no clear relationship between salt stoichiometry and the temperatures of the transitions. For anions with the same charge, T_g or T_m decreased in the order, [2,6-NDC] > [1,4-BDC] and [Trim] > [Cit]. This trend suggests that aromaticity and the larger π-surface extension of the anion, together with its symmetry and rigidity, impart higher structural order.

Gelation tests

The gelating ability of the salts was tested in water, conventional organic solvents and ionic liquids. The resistance to flow of the gels, such as those shown in Figure 1, was tested by the tube inversion test.[19] On this basis, the white opaque gels were stable for almost three months at room temperature in sealed vessels.

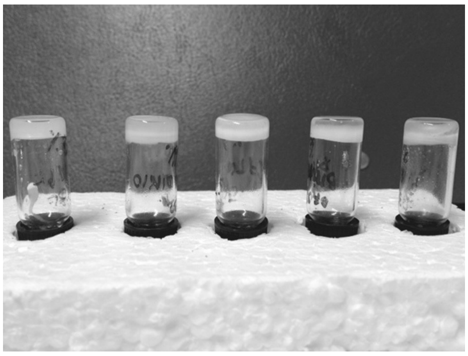

Figure 1. Gel phases at 5 wt % formed by (from left to right) [p-C_{12}im][1,4-BDC]/glycerol, [p-C_{12}im]$_2$[EDTA]/glycerol, [p-C_{12}im][1,4-BDC]/[bmim][BF_4], [p-C_{12}im]$_3$[Trim]$_2$/[bmim][BF_4] and [p-C_{12}im]$_3$[Cit]$_2$/[bmim]BF_4].

Organic solvents

Tables 1 and S2 and S3 (the Supporting Information) summarize the results from gelation tests performed on a range of conventional organic solvents with different polarities and hydrogen-bond donor abilities. Table 1 also includes the tempera-

Table 1. Values of CGC, T_{gel} and ΔH_m for organogels.[a]

	Solvents					
	Glycerol				Octanol	
	CGC[b]	T_{gel}[c]	T_{gel}[d]	ΔH_m[g]	CGC[b]	T_{gel}[c]
[p-C_{12}im][1,4-BDC]	3.2	37.2	36.2			
			42.6[e]	1.8		
[p-C_{12}im] [2,6-NDC]	2.3	31.9	33.8			
			57.0[f]	–		
[p-C_{12} im]$_2$[EDTA]	2.0	SM	SM		5.0	33.0
			41.4[e]	3.6		ns
[m-C_{12}im] [1,4-BDC]	3.7	23.7	27.6			
			ns			
[m-C_{12}im]$_2$[EDTA]	2.0	24.0	27.3			
			29.3[e]	0.5		

[a] Appearances: SM = soft material; ns = no detectable DSC endotherm on heating. [b] %, w/w gelator/solvent. [c] T_{gel} values (°C) were reproducible within 1 °C; T_{gel} values determined at the CGC by the falling-ball method. [d] T_{gel} values (°C) were reproducible within 1 °C; T_{gel} determined at 5 wt % of gelator by the falling ball method. [e] T_{gel} values (°C) determined by DSC. [f] T_{gel} value (°C) for a glass transition determined by DSC. [g] ΔH_m (J g^{-1}) determined by DSC.

tures corresponding to the gel-sol transitions (T_{gel}) at both 5 wt% and the critical gelation concentrations (CGC). The salts are soluble in polar, protic solvents and insoluble in polar aprotic ones. Some of the salts were able to gelate glycerol and 1-octanol, and some of the gels were classified as soft materials (SM) because they were stable to the tube inversion test, but were unable to support a lead ball (see below).

Irrespective of the isomeric cation, the CGCs reported in Table 1 decrease with increasing π-surface area of the anion ([1,4-BDC] > [2,6-NDC]) and changing from divalent aromatic anions to tetravalent aliphatic anions ([2,6-NDC] > [EDTA]).

As noted above, we also determined the thermal stabilities (T_{gel}) of gels at 5 wt% gelator concentrations using data from both the falling-ball method and DSC measurements. Thermograms corresponding to gel–sol transitions are reported in Figure S3 (the Supporting Information). They exhibit large changes in the heat capacities associated with second-order phase transitions. All measurements were made in triplicate to verify thermoreversibility and reproducibility. However, the second run was measured 24 h after the first because gel reformation was slow. As expected, T_m values for neat gelators (the Supporting Information, Table S1) and T_{gel} values for the corresponding organogels (Table 1) are very different; the media into which the melting solids dissolve are not comparable.

DSC data for neat gelators are consistent with the observation that the thermal stability of the gel phases is dependent on the isomer of the cation employed to make a salt. For both the [EDTA]- and [1,4-BDC]-derivatives, thermal stability was higher for the *para* than the *meta* cations; differences in the isomeric nature of the cation affect packing in the neat solids as well as in the gel SAFINs. However, the thermal stability of the gels appears to be enhanced by the increase in π-surface area of the anions associated with the *para* isomers: the T_{gel} values for the [1,4-BDC]- and [2,6-NDC]-salts are 42.6 and 57.0 °C, respectively.

Ionic liquids

Gelation tests were performed also using ILs as the solvents (the Supporting Information, Table S4). With the exception of $[m\text{-}C_{12}im]_3[Cit]_2$, all of the salt gelators were able to gelate $[bmim][BF_4]$ and the CGC values were higher than with conventional organic solvents. Whereas *para* isomers gelated most of ILs tested, *meta* isomers precipitated or formed gelatinous precipitates.

Gelation of ILs by salts, especially those with different anions, raises an important question: What is the nature of the gelator? Specifically, do the anions remain with their original cations? To answer this question, systems in which two cations and two anions (one set from the gelator and the other from the IL) were mixed and their gelation characteristics were compared with those from the ionogel $[p\text{-}C_{12}im]_3[Cit]_2/[bmim][NTf_2]$ (CGC = 2.6%) as well as salts derived from exchange processes, ($[p\text{-}C_{12}im][NTf_2]_2$ and $[bmim]_3[Cit]$). The mixtures of $[p\text{-}C_{12}im][NTf_2]_2$ and $[bmim]_3[Cit]$ were prepared at the same cation and anion mole ratios as those in the ionogel ($n_{[bmim+]}/n_{[p\text{-}C12im2+]} = 506$ and $n_{[NTf2]}/n_{[Cit]} = 72$). In both cases, heating and subsequent cooling of the mixtures did not induce soft materials formation. According to a previous report,[24] we centrifuged (6000 rpm, 1×10 min; 6000 rpm, 4×40 min) the $[p\text{-}C_{12}im]_3[Cit]_2/[bmim][NTf_2]$ gels to check for phase separation to solid and liquid components. However, the components of the gelatinous suspensions could not be separated. From these results and the non-gelating ability of $[p\text{-}C_{12}im][NTf_2]_2$ in $[bmim][NTf_2]$ (gelation tests were performed both at 2.6 and 5 wt%), it is possible to identify $[p\text{-}C_{12}im]_3[Cit]_2$ as the gelator. Additional support for this assertion was found in the very different transitions observed from DSC thermograms for $[p\text{-}C_{12}im][NTf_2]_2$, $[p\text{-}C_{12}im]_3[Cit]_2$ and $[bmim]_3[Cit]$ (the Supporting Information, Figure S2) and the one for the $[p\text{-}C_{12}im]_3[Cit]_2/[bmim][NTf_2]$ ionogel (Figure S4).

CGC values for gels in $[bmim^+]$-based ILs were lower for [1,4-BDC] than for [2,6-NDC] and for [Cit] than for [Trim], irrespective of the isomeric cation (3.4% and 4.3%, 3.5% and 5%, respectively). Although the number of examples is small, the data indicate that the gelation process is favored by a decrease in the aromatic character of the anion. Previously, similar behavior was observed for ionogel formation from some functionalized diimidazolium salts.[17] In that case (and in this one), the aromatic cation of the gelator preferably gelated ILs having an aliphatic cation. This suggests the benefit of structural complementarity between the gelator and IL solvent structures.

Data collected for [Trim], [Cit], and [EDTA]-based organic salts allow the effect of the IL anion structure on gel phase formation to be explored. Irrespective of the gelator considered, the largest CGC values were always observed in $[bmim][BF_4]$, the IL having the largest hydrogen-bond accepting ability, β ($\beta = 0.376$, 0.207, 0.243, 0.146 for $[bmim][BF_4]$, $[bmim][PF_6]$, $[bmim][NTf_2]$ and $[bmim][SbF_6]$ respectively).[25]

Gelation by LMWGs is the result of solvent entrapment within a 3D SAFIN. In our case, such a process should involve interactions between ions of the gelator and the solvent. Consequently, interactions between ions of the solvent and gelator should be favored when the β values are lower.

Also, as mentioned, data for $[p\text{-}C_{12}im]_3[Cit]_2$ and $[p\text{-}C_{12}im]_2[EDTA]$ in $[bmim][NTf_2]$ and $[bmpyrr][NTf_2]$ suggest that decreasing the aromatic character of an IL cation leads to higher CGC values. In that regard, T_{gel} values at the CGC and 5 wt% gelator concentrations were collected (Table 2 and the Supporting Information, Figure S4).

Some of the ionogels were "soft materials". Their T_{gel} values ranged from 22.2 to 53.0 °C and, similarly to organogels, values determined using DSC measurements were higher than those from the falling-ball method. Furthermore, according to data collected for organogels and the corresponding neat salts, T_{gel} values were higher for ionogels formed by *para* isomers than *meta* ones. In $[bmim][BF_4]$ as the solvent, only minor differences in thermal stability were detected as a function of the anion nature with the *meta* and *para* isomers of the cation, and T_{gel} increased slightly on going from bivalent to trivalent anions.

Data for [Trim]- and [Cit]-based gelators show that T_{gel} decreases as: $[bmim][BF_4] > [bmim][PF_6] > [bmim][SbF_6] > [bmim]$

Table 2. T_{gel} and ΔH_m values for ionogels at 5 wt % gelator concentrations.[a]

Ionic liquids	[*p*-C$_{12}$im] [1,4-BDC] T_{gel}[b]	 ΔH_m[e]	[*p*-C$_{12}$im] [2,6-NDC] T_{gel}[b]	 ΔH_m[e]	[*p*-C$_{12}$im]$_3$ [Trim]$_2$ T_{gel}[b]	 ΔH_m[e]	[*p*-C$_{12}$im]$_3$ [Cit]$_2$ T_{gel}[b]	 ΔH_m[e]	[*p*-C$_{12}$im]$_2$ [EDTA] T_{gel}[b]	 ΔH_m[e]
[bmim][PF$_6$]					41.4 64.3[c]	1.9	SM 67.1[c]	2.1	56.8 65.0[c]	0.7
[bmim][NTf$_2$]					41.7 44.2[c]	2.7	42.4 49.5[c]	5.2	42.0 45.3[c]	2.9
[bmim][BF$_4$]	53.4 81.7[c]	1.9	SM 84.7[c]	1.9	47.9 85.1[c]	1.3	49.5 85.4[c]	1.7	89.0 ns	–
[bmim][SbF$_6$]					43.7 49.8[c]	1.2	39.9 50.3[c]	2.2	49.0 ns	–
[bmpyrr][NTf$_2$]	36.3 39.2[d]	–					42.8 49.1[c]	2.6	47.0 44.6[c]	1.7
Ionic liquids	[*m*-C$_{12}$im] [1,4-BDC] T_{gel}[b]	 ΔH_m[e]	[*m*-C$_{12}$im] [2,6-NDC] T_{gel}[b]	 ΔH_m[e]	[*m*-C$_{12}$im]$_3$ [Trim]$_2$ T_{gel}[b]	 ΔH_m[e]	[*m*-C$_{12}$im]$_3$ [Cit]$_2$ T_{gel}[b]	 ΔH_m[e]	[*m*-C$_{12}$im]$_2$ [EDTA] T_{gel}[b]	 ΔH_m[e]
[bmim][PF$_6$]					39.9 62.0[c]	2.1	35.4 62.4[c]	1.9	34.7 ns	
[bmim][NTf$_2$]										
[bmim][BF$_4$]	SM 47.2[c]	1.5	28.4 47.4[c]	2.0	SM 50.6[c]	2.5			53.0 53.9[c]	1.0
[bmpyrr][NTf$_2$]					28.2 65.9[d]	–	SM 60.5[d]	–		

[a] SM = soft material. ns = no discernible DSC endotherm. [b] T_{gel} values (°C) were reproducible within 1 °C; T_{gel} at 5 wt % of gelator by falling-ball method. [c] T_{gel} values (°C) were reproducible within 1 °C; T_{gel} at 5 wt % gelator using DSC thermograms. [d] For glass transition from DSC thermograms. [e] ΔH_m (J g$^-$) from DSC thermograms.

[NTf$_2$] > [bmpyrr][NTf$_2$]. This order is not the one expected on the basis of the anion coordination ability of the ILs ([BF$_4$] > [SbF$_6$] > [NTf$_2$] > [PF$_6$]).[25] Rather, the IL anion symmetry appears to be the more important factor.

In general, data collected using [*p*-C$_{12}$im]$_3$[Cit] and [*p*-C$_{12}$im]$_2$[EDTA] as gelator also show slightly higher thermal stabilities for ionogels formed in [bmim][NTf$_2$] than in [bmpyrr][NTf$_2$].

POM measurements

The gel phases were characterized further by several techniques. In some cases, attempts to record POM images of gels with 5 wt % of gelator between glass slides (Figures 2 and S5) were unsuccessful because the pressure applied to the glass while preparing the samples disrupted the SAFIN.

Comparisons of the images indicate that the nature of both the solvent and the cation affected the morphologies. A clear example is shown by the glycerol and octanol gels of [*p*-C$_{12}$im]$_2$[EDTA] (Figures 2 a,b). A very thick network is observed in glycerol whereas spherulitic domains are found in octanol. On the other hand, the gels of [*p*-C$_{12}$im^{2+}] and [*m*-C$_{12}$im^{2+}]-based salts with EDTA as the anion and glycerol as the solvent were tangled fibrous systems (Figures 2 a,c).

Three distinct morphologies were identified for the ionogels: 1) thick textures, 2) spherulitic networks, and 3) reticular textures. The actual morphology seems to be determined principally by the nature of gelator anion rather than the isomer of the cation. Based on comparisons of the images in Figures 2 d and S5 b,c, Figures 2 f and S5 o, Figures 5 d,e, Figures 2 h,i, and Figures S5 n and S5 f, the morphologies were the same when only the cationic part of the gelator, [*m*-C$_{12}$im^{2+}] or [*p*-C$_{12}$im^{2+}], differed.

However, the morphology of the gels was very dependent on the specific IL employed. Using [*p*-C$_{12}$im]$_3$[Cit]$_2$ as the gelator, the images indicate that the gel networks were affected especially by the symmetry of the IL anion. With the tetrahedral anion, [BF$_4$], a reticular network was observed (Figure 2 g); with the octahedral anions, [PF$_6$] and [SbF$_6$], thick textures characterized by spherulitic domains were found (Figure 2 d and S5 j). In addition, as indicated by the values of T_{gel} reported in Table 2, increasing anion symmetry increased the ionogel stability.

Finally, with the same IL as solvent, ([bmim][BF$_4$]), reticular networks were detected for gels with [*p*-C$_{12}$im][1,4-BDC] and [*p*-C$_{12}$im]$_3$[Cit]$_2$ (Figures S5 n and 2 g), whereas spherulitic domains could be observed in gels with ([2,6-NDC]-, [Trim]- and [EDTA]-based salts (Figures S5g, S5 o and 2 h, respectively).

Mechanical properties

Mechanical properties of both organo- and ionogels were investigated at room temperature using rheology and a frequency of 1 Hz for strain sweeps and strains from 0.02 % to 0.5 % for frequency sweeps; the values were chosen to be within the linear viscoelastic region (LVR) of the gels. In all strain sweeps, G' was higher than G'' at low values of strain, indicating a solid-like behavior, and $G' < G''$ at higher strains, indicating liquid-like behavior. Furthermore, at the strain values employed for frequency sweeps, (γ), G' was always higher than G''. These observations support the gel nature of the samples.[26] A measure of the gels strength was extracted from the crossover points of yield strain (γ; i.e., where G'' becomes equal to G') and the loss tangents ($\tan\delta = G''/G'$). Indeed, they represent the level of stress needed to detect the flow of material and strength of colloidal forces operating in the gel networks. In general, the increase in gel strength induces a decrease in tan δ and a corresponding increase in γ.

Organogels

The rheology data are reported in Figure S6 and Table 3. No rheological investigations were conducted for gels of [*p*-C$_{12}$im]$_2$[EDTA] or [*m*-C$_{12}$im][1,4-BDC] in glycerol because of their low thermal stability and one of them being a soft material (Table 1).

Tan δ values ranged from 0.18 for [*p*-C$_{12}$im]$_2$[EDTA]/octanol to 0.77 for [*m*-C$_{12}$im]$_2$[EDTA]/glycerol gels. Values less than 1 suggest SAFINs with strong association among particles. According to γ values and as accounted for by the increase in

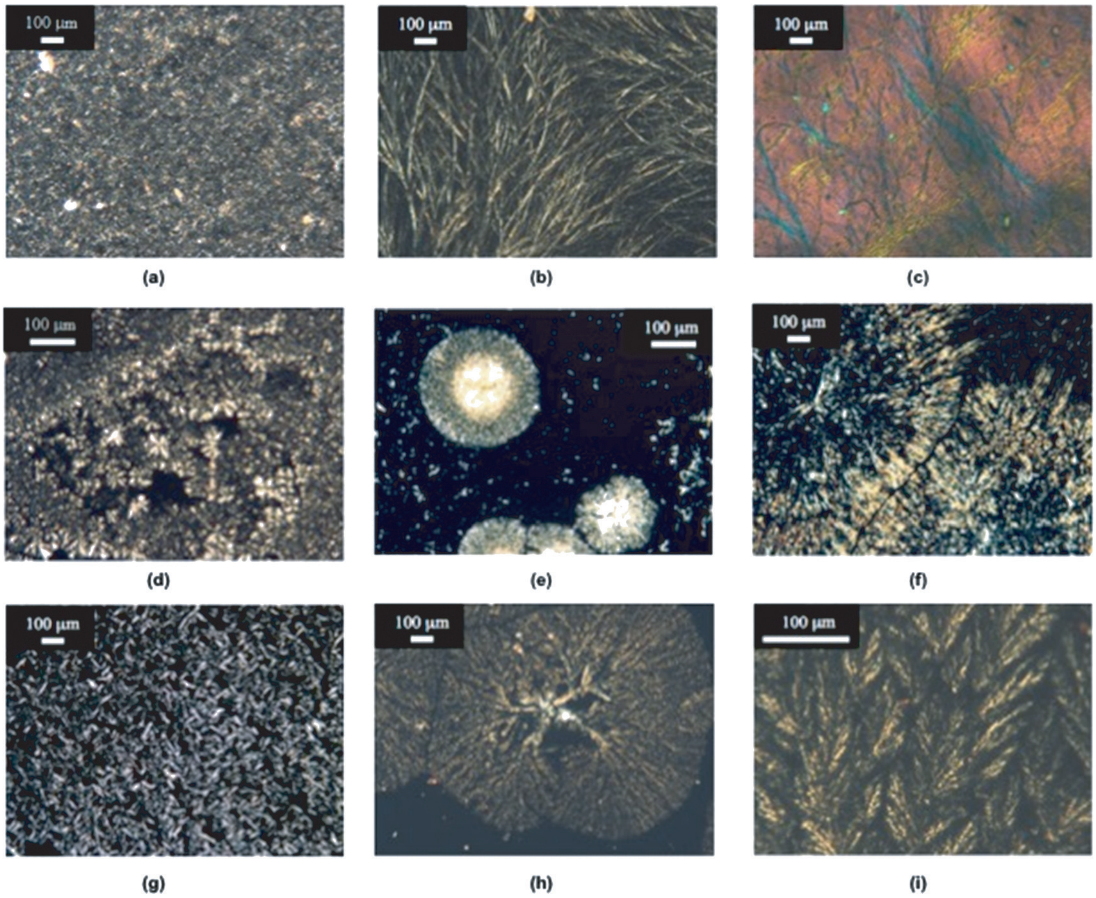

Figure 2. POM images of organogels and ionogels at 5 wt%; a) [p-C$_{12}$im]$_2$[EDTA] in glycerol at room temperature; b) [p-C$_{12}$im]$_2$[EDTA] in octanol at room temperature after first heating and cooling of the sample; c) [m-C$_{12}$im]$_2$[EDTA] in glycerol at room temperature after first heating and cooling of the sample; d) [p-C$_{12}$im]$_3$[Cit]$_2$ in [bmim][PF$_6$] at room temperature after first heating and cooling of the sample; e) [m-C$_{12}$im]$_3$[Trim]$_2$ in [bmim][PF$_6$] at 40 °C of cooling ramp of the sample after first heating; f) [m-C$_{12}$im]$_3$[Trim]$_2$ in [bmim][BF$_4$] at room temperature after first heating and cooling of the sample; g) [p-C$_{12}$im]$_3$[Cit]$_2$ in [bmim][BF$_4$] at room temperature; h) gel of [p-C$_{12}$im]$_2$[EDTA] in [bmim][BF$_4$] at 40 °C after first heating and cooling of the sample; i) [m-C$_{12}$im]$_2$[EDTA] in [bmim][BF$_4$] at room temperature.

Table 3. G' and G'' at $\gamma = 0.05\%$, $\tan\delta = G''/G'$ and values of γ at $G'' = G'$ for gels investigated at 5 wt% gelator concentrations and 25 °C. Error limits are based on average of three different measurements with different aliquots.

Gel	G' [Pa]	G'' [Pa]	$\tan\delta$	γ at $G'' = G'$
[p-C$_{12}$im][1,4-BDC]/glycerol	16 900 ± 400	6630 ± 130	0.39 ± 0.01	4.8 ± 0.2 %
[p-C$_{12}$im][2,6-NDC]/glycerol	3340 ± 330	1830 ± 70	0.55 ± 0.02	0.2 ± 0.1 %
[m-C$_{12}$im]$_2$[EDTA]/glycerol	5350 ± 650	4150 ± 460	0.77 ± 0.01	4.3 ± 0.2 %
[p-C$_{12}$im]$_2$[EDTA]/octanol	9940 ± 640	1850 ± 370	0.18 ± 0.06	2.2 ± 0.1 %
[p-C$_{12}$im][1,4-BDC]/[bmim][BF$_4$]	4340 ± 220	590 ± 80	0.14 ± 0.01	3.2 ± 0.6 %
[p-C$_{12}$im][2,6-NDC]/[bmim][BF$_4$]	2200 ± 800	300 ± 100	0.13 ± 0.02	36 ± 5 %
[p-C$_{12}$im]$_3$[Trim]$_2$/[bmim][BF$_4$]	840 ± 50	120 ± 10	0.14 ± 0.01	21 ± 2 %
[p-C$_{12}$im]$_3$[Cit]$_2$/[bmim][BF$_4$]	303 ± 14	55 ± 15	0.18 ± 0.06	7.4 ± 1.2 %
[p-C$_{12}$im]$_2$[EDTA]/[bmim][BF$_4$]	1500 ± 700	260 ± 70	0.16 ± 0.01	32 ± 9 %
[m-C$_{12}$im][1,4-BDC]/[bmim][BF$_4$]	20 200 ± 4700	4400 ± 700	0.22 ± 0.02	6.9 ± 1.4 %
[m-C$_{12}$im][2,6-NDC]/[bmim][BF$_4$]	19 800 ± 7500	5800 ± 800	0.29 ± 0.03	15 ± 3 %
[m-C$_{12}$im]$_3$[Trim]$_2$/[bmim][BF$_4$]	28 000 ± 4600	4980 ± 550	0.180 ± 0.001	0.5 ± 0.3 %
[m-C$_{12}$im]$_2$[EDTA]/[bmim][BF$_4$]	3600 ± 600	840 ± 90	0.23 ± 0.01	1.0 ± 0.4 %
[p-C$_{12}$im]$_3$[Trim]$_2$/[bmim][PF$_6$]	6630 ± 870	850 ± 120	0.13 ± 0.02	6 ± 1 %
[p-C$_{12}$im]$_3$[Cit]$_2$/[bmim][PF$_6$]	8400 ± 900	1410 ± 90	0.17 ± 0.04	15 ± 3 %
[p-C$_{12}$im]$_2$[EDTA]/[bmim][PF$_6$]	3340 ± 560	350 ± 30	0.11 ± 0.01	3.4 ± 0.1 %
[m-C$_{12}$im]$_3$[Trim]$_2$/[bmim][PF$_6$]	3340 ± 340	370 ± 90	0.11 ± 0.02	1.7 ± 0.3 %
[m-C$_{12}$im]$_3$[Cit]$_2$/[bmim][PF$_6$]	1390 ± 20	270 ± 20	0.19 ± 0.02	0.4 ± 0.1 %
[m-C$_{12}$im]$_2$[EDTA]/[bmim][PF$_6$]	1400 ± 300	250 ± 60	0.18 ± 0.01	4.6 ± 1.2 %

tan δ values on going from [p-C_{12}im][1,4-BDC] to [p-C_{12}im][2,6-NDC], gel strength decreased with the increase in π-surface area of the gelator anion. Another indicator of gel strength is T_{gel}. Interestingly, the decreases of T_{gel} values of organogels in glycerol correlate with the rise in tan δ values.

Ionogels

Viscoelastic properties of the IL solvents could, in principle, contribute to gelation in the ionogels. However, the mechanical properties of the most viscous IL employed, [bmim][PF_6], were those of a classical Newtonian liquid. Consequently, the mechanical properties of the ionogels are attributed to the interactions of both components. To compare the effects of structural changes within the solvent portion, the rheological properties of gels with [bmim][BF_4] and [bmim][PF_6] were investigated (Figure 3 and Table 3).

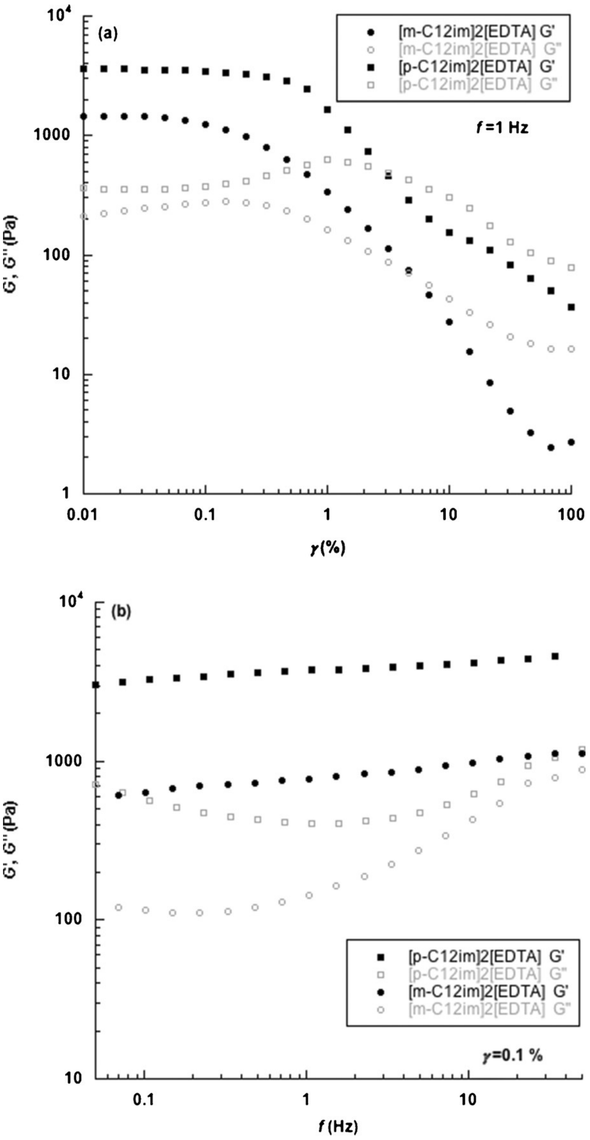

Figure 3. Strain (a) and frequency (b) sweep plots for ionogels obtained in [bmim][PF_6] at 5 wt % gelator and 25 °C.

For an analogous reason, the rheological properties of gels consisting of [p-C_{12}im]$_3$[Cit]$_2$ and different ILs were investigated (the Supporting Information, Figure S7).

The tan δ values, from 0.11 for [p-C_{12}im]$_2$[EDTA]/[bmim][PF_6] to 0.29 for [m-C_{12}im][2,6-NDC] in [bmim][BF_4], are lower than the ones corresponding to organogels. They indicate that stronger gels were formed in the IL solvents than in organic solvents. A similar trend has been recently detected by Schalley et al. for a crown-ether functionalized bisurea gelator.[27]

Data reported in Table 3 show that tan δ and γ are affected by the structures of both the solvent and gelator. Although the differences in tan δ values are small, the ionogels from the *para* cation of the gelator are stronger than those from the *meta*. This conclusion is consistent with the changes in the γ values. Interactions are stronger among gelator molecules with the *para* isomer than with the *meta*.

More complex behavior was detected when the gelator anion was varied. Indeed, γ values determined in [bmim][BF_4] indicate that increased aromatic character of the anion leads to stronger gels: ionogel strength increases between [1,4-BDC] and [2,6-NDC] and between [Cit] and [Trim]. However, the effect of the anion in [bmim][PF_6] solvent depended on the isomer of the cation of the gelator. In general, and as found for the organogels, the results with ionogels indicate that higher rigidity and symmetry in both the cationic and anionic parts of the gelator aid gel strength and thermal stability.

Table S5 summarizes data about γ and tan δ for ionogels with [p-C_{12}im]$_3$[Cit]$_2$ and different IL solvents.

The γ values decrease in the order: [bmim][PF_6] > [bmim][BF_4] > [bmim][SbF_6] > [bmpyrr][NTf_2] > [bmim][NTf_2]. On the other hand, analysis of tan δ values indicates that the weakest gel was formed in [bmim][NTf_2] solution. This trend may depend on the flexibility of the ionogel SAFINs. As discussed above, increased symmetry of the IL anion seems to favor spherulitic domains that should impart higher strength than the other SAFIN types to the ionogels. However, G' measured in [bmim][BF_4] was lower than in [bmim][NTf_2]. In an attempt to explain the trend, we also considered the anion coordination ability (β), polarity and viscosity (the Supporting Information, Table S6). The two latter parameters have been used to interpret results of gelation tests with organic solvents.[28] Of these, viscosity appears to be the most important factor; its decrease ([bmim][PF_6] > [bmim][BF_4] > [bmim][SbF_6] > [bmim][NTf_2]) is in the same order as the values of γ. Furthermore, among the ILs investigated, [bmim][NTf_2] forms ionogels that flow most easily. This may possibly be related to the low cross-linking ability of the NTf_2 anion.[29]

Finally, comparison between tan δ and γ values of ionogels with [bmim][NTf_2] and [bmpyrr][NTf_2] as the solvent suggest that the aliphatic cation aids more gel strength.

Thixotropic and sonotropic behavior

Many reports have focused on creating thixotropic organogels because they may be useful in several applications.[30] Examples of thixotropic organometallic LMWGs as well as toluene gels with *N*-(3-hydroxypropyl)-dodecanamide or silicone oil gels of (*R*)-12-hydroxyoctadodecanamide have been reported.[31] Thus, the ability of our ionogels to regain their viscoelastic properties after applying destructive strain from magnetic stirring or ultrasound irradiation were explored.

Surprisingly few ionogels have been shown to be thixotropic. In these cases, their self-repairing ability was advantageous for enhancing quasi-solid-state DSSC performance[32] and for improving solid-like lubricants.[14] Furthermore, to the best of our knowledge, the effect of ultrasound irradiation on the stability of ionogels has not been exploited extensively. We have recently reported the thixotropic and sonotropic behavior of ionogels formed by some functionalized diimidazolium salts.[17] Data for the ionogels investigated here are reported in Table S7 (the Supporting Information).

Firstly, gel phases were subjected to magnetic stirring (at 1000 rpm for 5 minutes). With few exceptions (6 cases out of 22), gels reformed qualitatively after the samples were stored at 4 °C overnight. The non-thixotropic gels showed the highest thermal stability. We have recently detected a similar behavior studying the thixotropic properties of two-component gels formed by some diimidazolium salts in the presence of aromatic guests.[33] Based upon the results found here, thixotropic recovery is enhanced when the SAFIN consists of a more flexible fibrous or spherulitic network in which network interactions may be weaker.

The thixotropic behavior of the ionogels was also analyzed more quantitatively by rheology. Gels were subjected initially to conditions within the LVR ($\gamma = 0.05$–0.1% and $f = 1$ Hz). Thereafter, destructive strain was applied ($\gamma = 5$–50% and $f = 1$ Hz). The evolutions of G' and G'' after cessation of the destructive strain applying the strain are displayed in Figures 4 and S8 (the Supporting Information). In general, at least two destruction–recovery cycles were performed on each sample. Although the level of recovery was not complete in any of the samples, G' values higher than G'' values, demonstrating the presence of a gel, were found after applying strain levels in the viscoelastic region.

The percentage of recoveries indicated in Table S7 (the Supporting Information) range from 0% to 15% in [*m*-C_{12}im]$_2$[EDTA]/[bmim][BF_4] to 73% in [*p*-C_{12}im]$_3$[Cit]$_3$/[bmim][NTf_2].

In some cases, G' continued to rise over long periods (labeled as "G' increasing" in Table S7) or oscillated with time (labeled as "oscillations" in Table S7). These behaviors did not allow the percent of recovery to be determined. The oscillatory behavior is especially bizarre. However, it was found on several different samples prepared independently, with different amounts of gels between the rheometer plates, and when measurements were made on a different rheometer and with plate–plate or cone–plate tool geometries.

Nandi et al.[34] have reported similar oscillatory behavior for the moduli of gels. They ascribed the oscillations to a shear-assisted re-aggregation process. That explanation seems logical here as well. It could give rise to a different organization of the gel network. Similar considerations have been made in consideration of kinetic rheological and opacity measurements (see below).

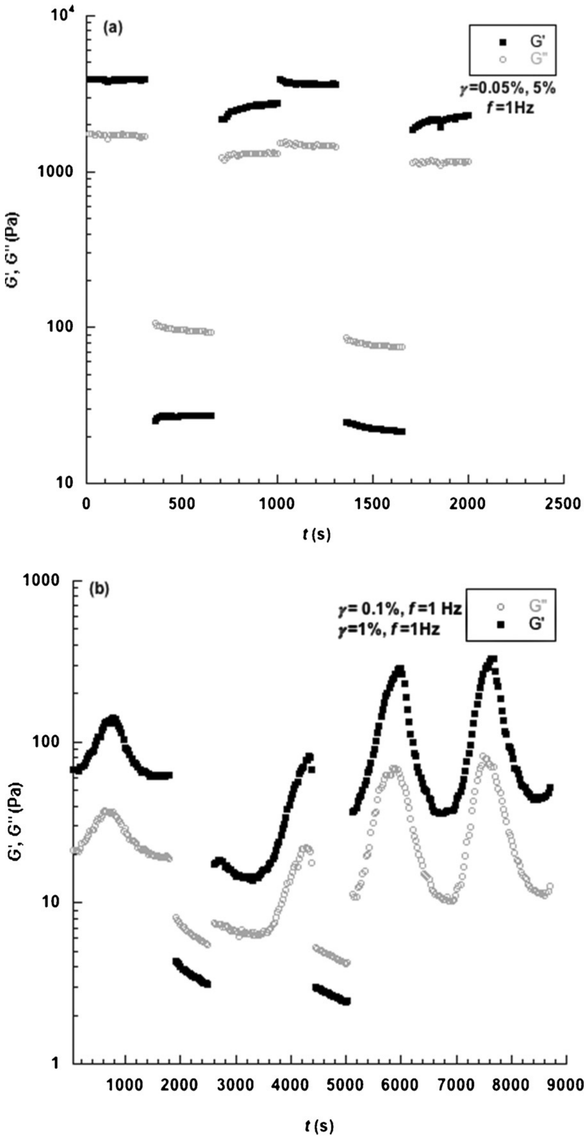

Figure 4. G' and G'' at 25 °C as a function of time and application of low (G' G'' regimes) and destructive stain ($G'' > G'$ regimes) to (a) [*p*-C_{12}im]$_3$[Cit]$_2$/[bmim][NTf_2] and (b) [*p*-C_{12}im]$_3$[Cit]$_2$/[bmim][BF_4] samples at 5 wt% of gelator concentrations.

As stated above, the sonotropic behavior of the ionogels was also explored. Results collected are displayed in and they allow distinguishing three different situations. In 5 out 22 gels irradiated, ultrasound led to loss of viscoelasticity (the Supporting Information, Table S7); in 12 gels, irradiation did not affect qualitatively the consistency of the samples; all of the 5 soft materials were sonotropic. The sonotropic behavior was observed predominantly for *meta* isomers of the gelator cation bearing an aromatic anion. These materials also exhibit medium or low thermal stabilities and mostly spherulitic SAFINs (the Supporting Information, Figures S5 n, 2 f and 2 g).

Kinetic study of gel phase formation: rheology measurements

The kinetics of both organo- and ionogels formation were studied as a function of the time by rheology. Gelation by LMWGs can be described as a sequence of a stochastic nucleation events followed by growth of branched or unbranched fibers and their entanglement or physical interaction to form a 3D network (the SAFIN). The above processes have been treated using the Avrami equation.[35] This equation was initially developed to describe the crystallization of polymer and other melts. However, it is frequently used in its log–log form [Eq. (1)] to study gelation processes at a constant temperature:

$$\ln\left[-\ln(1-\Phi)\right] = \left[n\ (\ln k + \ln t)\right] \tag{1}$$

In which k is a rate constant, n is the so-called Avrami exponent that is associated with the type of growth leading to the SAFIN, t is time and Φ, the volume fraction of gel, can be calculated by the storage modulus at times 0 (i.e., when the aggregation is first noted by an increase in G'), t and ∞ (i.e., when G' reaches a maximum, plateau value) [Eq. (2)].

$$\Phi = (G'_{(t)} - G'_{(0)})/(G'_{(\infty)} - G'_{(0)}) \tag{2}$$

The rheological kinetic measurements were carried out within the LVR, using a low strain ($\leq 1\%$) and the data are shown in Figures 5, S9 and S10 (the Supporting Information).

As mentioned above, it was possible to perform rheological measurements only for organogels of [p-C_{12}im]$_2$[EDTA]/octanol because the gel phases in glycerol using [p-C_{12}im][1,4-BDC] and [p-C_{12}im][2,6-NDC] formed too slowly for $G_{(\infty)}$ to be evaluated. For the [p-C_{12}im]$_2$[EDTA]/octanol gel, values of k ($=0.70\times 10^{-3}\ s^{-2}$) and $n=1.89$ were calculated. In particular, $n=2$ predicts the two-dimensional or rod-like growth of the SAFIN (as is found in the POM images; Figure 2 b).

For reason described previously,[34] $G_{(\infty)}$ values could not be obtained in some experiments with ionogels, and therefore, Avrami analyses were not possible. With the exception of gelation by [p-C_{12}im][2,6-NDC], [p-C_{12}im]$_2$[EDTA] and [m-C_{12}im]$_2$[EDTA] in [bmim][BF_4], plots of the ionogel data for which Avrami plots are possible (Table 4 and the Supporting Information, Figure S10) show an induction period, indicative of slow, elementary nucleation steps.[36] Induction periods were also detected by RLS (see below).

In most cases, the Avrami exponent predicts two-dimensional growth of the network, consistent with the spherulitic or reticular objects observed in the POM images (Figures 2 g, S5 n–o and S5 m). However, $n=3$ is calculated for the [p-C_{12}im]$_3$[Cit]$_2$/[bmim][PF_6] ionogel. The POM image in Figure 2 d is consistent with the predicted growth of 3D objects in the SAFIN.

The values of k indicate that the rate of gel phase formation is not affected by the nature of the IL anions (see entries 4 and 5 in Table 4). On that basis, it appears from the experiments with [p-C_{12}im][1,4-BDC] that gel formation is slower when the ILs have an aliphatic cation (see entries 1 and 2 in Table 4). Ob-

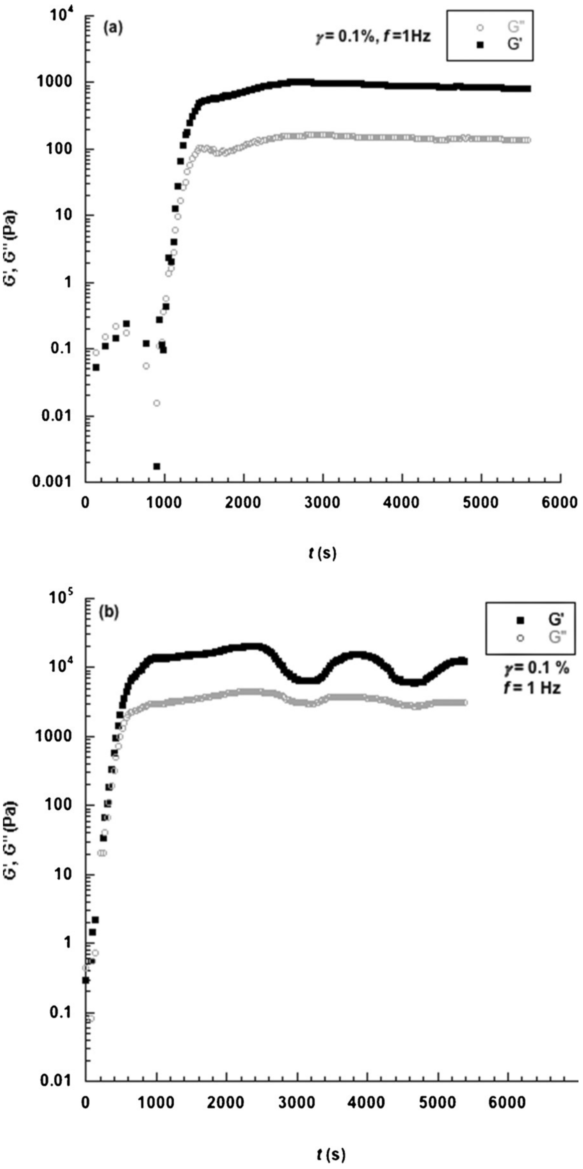

Figure 5. Plots of G' and G'' as a function of time collected at 25 °C for: a) [p-C_{12}im]$_3$[Trim]$_2$/[bmim][BF_4] and b) [p-C_{12}im]$_3$[Cit]$_2$/[bmim][PF_6] gel phases at 5 wt % gelator concentrations.

Table 4. Rate constants (k) and kinetic order (n) of gel formation, derived from rheology data treated by the Avrami Equation (1).

Entry	Gel	k [s^{-n}]	n
1	[p-C_{12}im][1,4-BDC]/[bmpyrr][NTf_2]	0.75×10^{-3}	1.85
2	[p-C_{12}im][1,4-BDC]/[bmim][BF_4]	1.13×10^{-3}	2.02
3	[p-C_{12}im]$_3$[Trim]$_2$/[bmim][BF_4]	0.89×10^{-3}	1.59
4	[p-C_{12}im]$_3$[Cit]$_2$/[bmim][BF_4]	1.98×10^{-3}	2.09
5	[p-C_{12}im]$_3$[Cit]$_2$/[bmim][PF_6]	1.95×10^{-3}	3.00

viously, additional examples will be needed in the future to test the generality of these hypotheses.

Gel phase formation: RLS measurements

Ionogel phase formation was also investigated by RLS measurements. RLS, a technique that detects aggregates in solution, takes advantage of enhanced light scattering intensity observed at wavelengths of light absorbed by aggregates when strong coupling exists among their chromophores.[37] RLS measurements also provide an estimate of the size of the aggregates; other factors being constant, RLS intensity (I_{RLS}) is directly proportional to the square of aggregate volume.[37b,38] This technique has been used to study aggregation processes involving very different systems.[39] Recently, we have used it to follow gel phase formation.[17,18,40]

Measurements of I_{RLS} as a function of time were carried out here at 25 °C (Figures 6 and S11). As found by rheological measurements also, plots of I_{RLS} as a function of time for [m-C$_{12}$im][1,4-BDC]/[bmim][BF$_4$] and [p-C$_{12}$im]$_3$[Cit]$_2$/[bmim][SbF$_6$] show an induction period before aggregates become detectable.

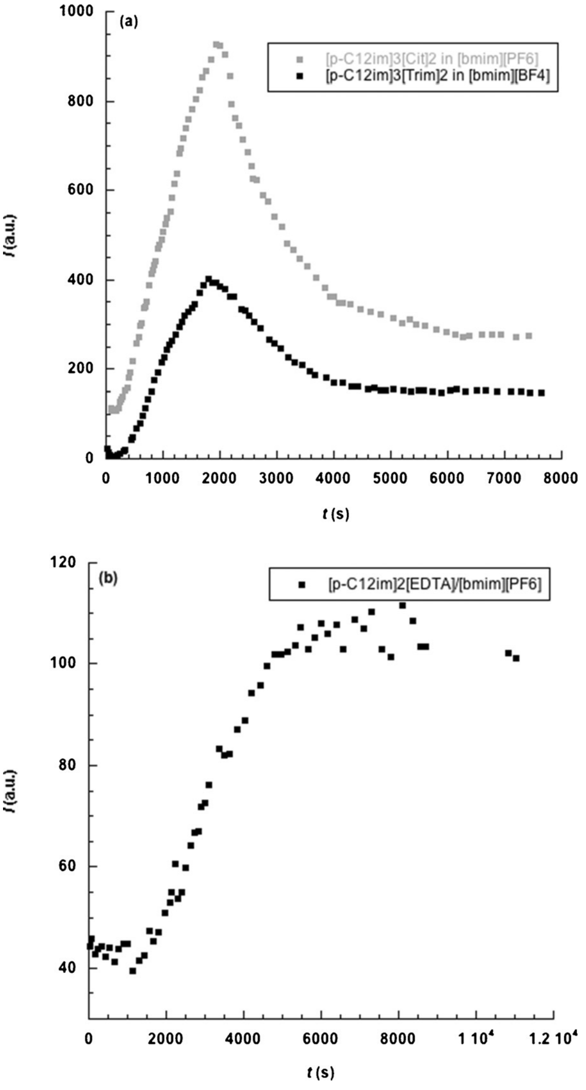

Figure 6. Plots of I_{RLS} as a function of time collected at 25 °C and corresponding to ionogels at 5 wt% gelator concentrations.

A careful analysis of the plots shows that gelation occurs through two different mechanisms that depend on the nature of the gelator and the IL solvent. Data corresponding to time and intensity of intermediate formation (t_m, I_m) and gelation (t_e, I_e) are collected in Table S8. The data in Figure 6 b indicate that gelation proceeds by a single step mechanism: I_{RLS} gradually increases with time until reaching a plateau value. The data in Figure 6 a are consistent with a two-step mechanism. There, I_{RLS} increases (I_m) and then decreases to a constant value (I_e), corresponding to the completion of gelation. This latter behavior has been previously reported using different techniques.[17,18,41] On this basis, and bearing in mind that the self-assembly process can involve fiber formation (i.e., 1D objects) before the 3D networks of SAFINs are completed, we attribute the increase and then decrease of the RLS intensity to initial formation of larger aggregates that subsequently rearrange into smaller and more stable ones. This is the opposite of Ostwald ripening, the normal manner in which SAFIN structures age!

Data collected in [bmim][BF$_4$] solvent shows that gelation times increase as the anions of the gelators are changed: [1,4-BDC] < [EDTA] < [Trim] < [Cit]. For trivalent anions, SAFIN networks evolved faster with the aromatic anion ([Trim]), but more extended aggregates were formed with the aliphatic anion ([Cit]) (the Supporting Information, Figures S5 o and 2 g).

With [1,4-BDC] as the common gelator anion and [bmim][BF$_4$] as the common solvent, a one-step mechanism for SAFIN formation was observed with [p-C$_{12}$im^{2+}] as the gelator cation and a two-step mechanism occurred with [m-C$_{12}$im^{2+}] (entries 1 and 9, Table S8). Furthermore, although the sizes of the aggregates are very similar ($I_{RLS} \approx 330$ a.u.), the cation structure affects gelation time significantly: $t_e = 600$ and 4700 s for [p-C$_{12}$im^{2+}] and [m-C$_{12}$im^{2+}], respectively. Although other interesting comparisons are available from the data in Table S8, but they depend upon small numbers of examples, their generality must be tested in future experiments.

Finally, the thermal reversibility of the gelation process of [p-C$_{12}$im]$_3$[Cit]$_2$/[bmim][BF$_4$] (i.e., are aggregates after consecutive heating–cooling cycles of comparable size?) was investigated using RLS measurements. Results from 3 cycles are displayed in Figure S11 (the Supporting Information). Gel formation occurred by a two-step mechanism and the times corresponding to gel phase formation as well as to the maximum I_{RLS} value gradually decreased between cycles. However, because the I_{RLS} and T_{gel} values after each cycle (49.5, 49.7 and 47.9 °C for the first, second and third cycle, respectively) were not affected by reheating and recooling, we conclude that the gels and their SAFINs remained virtually the same.

Opacity measurements

Gel phase formation was also investigated by recording the opacity of gelating samples at 568 nm (Abs$_{568\,nm}$) as a function of time (the Supporting Information, Figure S12).

Gel opacity can be related qualitatively to the number and the size of polydisperse nanostructures in a system, including the crystallinity of a gel.[41b] On that basis, there appears to be no significant changes in the crystallinity of gels with different gelators when [bmim][BF_4] was the solvent. Similarly, only small changes in the absorbance values were detected for gels with [*p*-C_{12}im]$_3$[Cit]$_2$ as the gelator and different ILs as the solvent.

However, significant changes in crystallinity were found when ionogels and organogels were compared. Abs$_{568\,nm}$ values increased on going from [*p*-C_{12}im]$_2$[EDTA]/octanol to [*p*-C_{12}im]$_2$[EDTA]/[bmim][BF_4] and [*p*-C_{12}im]$_2$[EDTA]/[bmim][PF_6] systems while crystallinity decreased on going from [*p*-C_{12}im][1,4-BDC]/[bmim][BF_4] to [*m*-C_{12}im][1,4-BDC]/[bmim][BF_4], indicating the importance of the isomer of the gelator cation.

Powder X-ray diffraction

Powder X-ray (PXRD) diffractograms of selected neat gelators and their 5 wt% gels are compared in Figures 7 and S13 (the Supporting Information). Spacings (*d*, nm) calculated from the Bragg relationship are collected in Tables S9–S13, as well. Ionogels formed in [bmim][PF_6] by the gelator consisting of the *para* isomer of the cation and three different anions were investigated to gain insight into the influence of the anion on molecular packing within the SAFINs (Figure S13). Also, the PXRD patterns for both [*p*-C_{12}im]$_2$[EDTA] and [*m*-C_{12}im]$_2$[EDTA] as neat solids and in [bmim][PF_6] gels were compared to determine whether the neat solid and SAFIN morphs differ and the role of the cation of the gelator on molecular packing within the SAFINs (Figures 7 and S13). Finally, packing within SAFINs of gels with [*p*-C_{12}im]$_2$[EDTA] as gelator and an IL ([bmim][PF_6]) or a "normal" solvent (glycerol) were compared (Figure 7).

The 2θ values of the diffraction peaks demonstrate that molecular packing of [*p*-C_{12}im]$_2$[EDTA] differs in its neat bulk solid, in its [bmim][PF_6] ionogel and in its glycerol organogel.[42] Also, the diffractograms of neat [*p*-C_{12}im]$_3$[Trim]$_2$, [*p*-C_{12}im]$_3$[Cit]$_2$, and [*m*-C_{12}im]$_2$[EDTA] differ from those of their gels with [bmim][PF_6] as the liquid. Thus, all the gelators investigated are polymorphic; the processes by which they aggregate and nucleate to form the 3D networks of their SAFINs depend acutely on the nature of the solvent–gelator interactions.

Although it was not possible to obtain diffraction quality single crystals of the gelators,[42b] we were able to assign possible cell constants and lattice types in some cases by indexing the PXRD peaks for the gelators and their gels (the Supporting Information, Table S14).[42a] At least 40 diffraction peaks were used to index each gelator, whereas 15–33 diffraction peaks were used for the gels. A few peaks with very low intensity could not be assigned; they may be from minor amounts of a different morph or trace impurities. Regardless, most of gelators and their gels pack in monoclinic lattices. As mentioned, the assigned unit cells for the gelators and those of the gels are different; the packing arrangements of the gelator molecules change significantly from the neat solid phase to their gel phases. Clearly, this observation constitutes a challenge to an even deeper understanding of how the SAFINs form from their sol phases, and points to an obvious direction for future investigations.

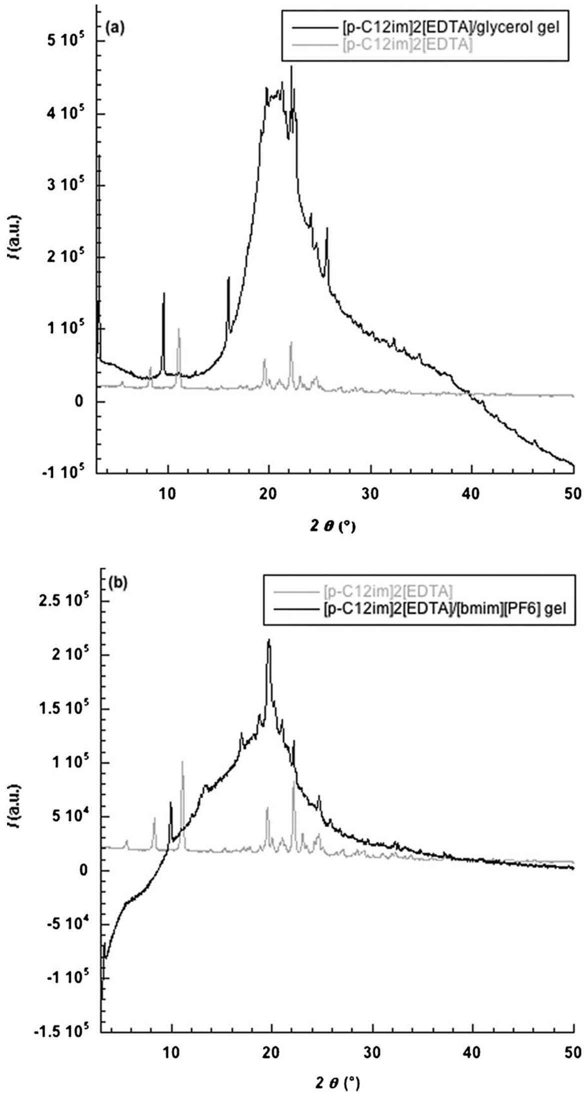

Figure 7. Diffractograms of neat gelators and of their 5 wt % gels in (a) glycerol and (b) [bmim][PF_6] after empirical background subtraction of the glycerol or [bmim][PF_6].

Although it is tempting to do so, we prefer not to use the PXRD data to speculate about details of the specific packing arrangements of the gelator molecules within their unit cells. However, all neat gelators show diffraction peaks that are consistent with (but not unique to) the presence of hydrogen bonding: $2\theta = 20.00^\circ$ (4.43 Å), 20.68° (4.29 Å), 20.14° (4.40 Å) and 20.92° (4.24 Å) for [*p*-C_{12}im]$_2$[EDTA], [*p*-C_{12}im]$_3$[Trim]$_2$, [*p*-C_{12}im]$_3$[Cit]$_2$ and [*m*-C_{12}im]$_2$[EDTA], respectively.[43] Also, a diffraction peak from [*p*-C_{12}im]$_3$[Cit]$_2$ at $2\theta = 25.08^\circ$ (3.63 Å) may be due to π–π stacking.[43–44]

The diffractograms of the organo- and ionogels contain peaks that may be due to self-assembly through hydrogen bonding interactions as well. Previously reported DFT calculations on some diimidazolium salts[18] indicate that the anions of the gelators may form bridges among diimidazolium cations.

As mentioned previously, the degree of additional stabilization of the gels by π–π interactions seems to depend on both the nature of the anion and the substitution pattern on the cation of the gelators. Indeed, irrespective of solvent nature, peaks at $2\theta = 25.70^\circ$ (3.46 Å) and 25.82 (3.54 Å) were observed for [*p*-C_{12}im]$_2$[EDTA] gels in both glycerol and [bmim][PF_6].

However, the gel of [*m*-C_{12}im]$_2$[EDTA] in [bmim][PF_6] lacks diffractions expected of π–π interactions and the gel of [*p*-C_{12}im]$_3$[Cit]$_2$ in [bmim][PF_6] exhibits diffraction peaks consistent with hydrogen bond formation only. Considering the non-aromatic nature of the [EDTA] anion, the occurrence of π–π interactions in [*p*-C_{12}im]$_2$[EDTA] must be ascribed to interactions among the cations. In general, the data indicate more facile bridging by [EDTA] than for the [Cit] anion. Also, DFT calculations[23] suggest a higher propensity for π-stacking by [*p*-C_{12}im^{2+}]. Finally, evidence for π-π interactions was also found in the diffraction peak of the [*p*-C_{12}im]$_3$[Trim]$_2$/[bmim][PF_6] ionogel at $2\theta = 25.83^\circ$ (3.53 Å), where both cation/cation and cation/anion interactions should be considered.

Conclusions

This work provides insights into the properties of gels formed by some diimidazolium salts. Interestingly, these gelators are able to gel solvents such as conventional solvents and ionic liquids which are frequently claimed for their very different properties. However, for both classes, solvents entrapped in the SAFIN are highly polar and viscous. According to rheological and opacity measurements, stronger and more crystalline gels are formed in the ILs than in organic solvents.

The properties of the ionogels seem to depend mainly on the nature of the IL solvent and of the gelator anion. These factors also affect the morphology and size of the aggregates characterizing the SAFINs as accounted for by POM images, RLS and opacity measurements.

Several gel phases show some thixotropic and sonotropic behavior, which may be both useful in view of future applications. The temporal changes in the SAFINs, followed by UV/Vis and RLS measurements, reveal significant differences in the gelation mechanisms when the structure of the gelator or IL anion are modified.

Finally, XRD diffractograms, collected for selected neat gelator and gel samples in glycerol and in [bmim][PF_6], have allowed hydrogen bond and π–π interactions to be identified as some of the forces stabilizing the gels and controlling the molecular packing arrangements within the SAFINs. In particular, the ability of the anion, whether aliphatic or aromatic, to connect cation planes appears to be a major driving force for gel stabilization.

Data collected demonstrate how small modifications of gelator structures and gelation solvents can modulate the properties of the soft materials. These, as a consequence of their strength and crystallinity, hold great promise in the construction of new DSSCs and electrochemical devices.

Experimental Section

Material and methods: Imidazole ($\geq$99%, Sigma–Aldrich), potassium hydroxide (99%, Fluka), α,α'-*p*-dibromoxylene (97%, Sigma–Aldrich), α,α'-*m*-dibromoxylene (97%, Sigma–Aldrich), 1-bromododecane (97%, Sigma–Aldrich), Amberlite IRA-400 resin (chloride form) (99.8%, Sigma–Aldrich), sodium hydroxide (99%, Fluka), 1,4-benzenedicarboxylic acid (98%, Sigma–Aldrich), 2,6-naphtalenedicarboxylic acid (97%, Sigma–Aldrich), trimesic acid (95%, Sigma–Aldrich), citric acid (99.5%, Fluka), ethylenediaminetetraacetic acid (98%, Sigma–Aldrich), acetonitrile (99.8%, Sigma–Aldrich), dichloromethane (99%, VWR), diethyl ether (99%, VWR) and all organic solvents used for gelation tests were analytical reagents used as received.

ILs as [bmim][NTf_2] (99%), [bmim][BF_4] (99%), [bmim][PF_6] (99%) were analytical reagents purchased from Iolitec and used as received, while [bmim][SbF_6] and [bmpyrr][NTf_2] were prepared and purified according to the reported procedures.[45]

^{1}H and ^{13}C NMR measurements were recorded on Bruker instruments of 300 and 400 MHz.

Melting points of products were measured by DSC. Precursor melting points were obtained on a Kofler melting point apparatus.

TGA measurements: TGA were performed on a TA 2910 differential scanning calorimeter interfaced to a TA Thermal Analyst 3100 controller while a slow stream of nitrogen flowed through the instrument cell. TGA measurements were performed equilibrating the sample at 25 °C, isothermal 0.1 min, afterwards using a temperature ramp with a rate of $10\,^\circ C\,min^{-1}$ from 25 °C to 300 °C.

DSC measurements: DSC was carried out on a DSC Q200 calorimeter (TA Instruments, New Castle, DE) interfaced to a TA Thermal Analyst 3100 controller connected to a RCS90 cooling system. Heating and cooling cycles were done in a $50\,mL\,min^{-1}$ stream of nitrogen. Samples were weighed ($\approx$5 mg for salts, $\approx$15 mg for gels) in T-zero aluminum pans. Transition temperatures from DSC are reported at the point of maximum heat flow.

After equilibration of the sample at 25 °C, DSC measurements of organic salts were performed heating the sample with a rate of $20\,^\circ C\,min^{-1}$ from 25 °C to 180 °C and cooling it with the same rate ramp to 0 °C. DSC measurements of gel phases were performed equilibrating the sample at 25 °C and using a temperature ramp with a rate of $10\,^\circ C\,min^{-1}$ from 25 °C to 100 °C and a cooling ramp to 0 °C.

Preparation of gels and T_{gel} determination: Gels were prepared by weighing into a screw-capped sample vial (diameter 1 cm) the amount of salt and solvent ($\approx$250 mg). The sample vial was heated in an oil bath at 90–95 °C until a clear solution was obtained. The vial was then cooled and stored at 4 °C overnight. The tube inversion test method was used to examine gel formation. To determine the T_{gel} values, a lead ball (weighing 46.2 mg and 2 mm of diameter) was placed on the top of the gel and the vial was put into a water bath. The bath temperature was gradually ($2\,^\circ C\,min^{-1}$) increased until the gel melted and the lead ball reached the bottom of the vial (T_{gel}). The T_{gel} values were reproducible within 1 °C.

POM measurements: Samples were casted between two glasses to record POM images. The samples were heated to their sol phases and cooled. The instrument used is a Leitz 585 SM-LUX-POL microscope equipped with crossed polarizers, a Leitz 350 heating stage, a Photometrics CCD camera interfaced to a computer, and an Omega HH503 microprocessor thermometer connected to a K (Chrome-Alome) thermocouple (Omega Engineering, Inc.).

Rheological measurements: Rheological measurements were recorded on an Anton Paar MCR 302 strain-controlled rheometer using a Peltier temperature controller and a cone plate (CP 25-2) tool, the sample was placed between the shearing plates of the rheometer. Rheological properties, such as strain sweep and frequency sweep, were recorded before and after heating the sample. Kinetics were performed in the linear-viscoelastic region, heating the sample to 90 °C for 30 min to ensure the formation of solution, then it was cooled at $\approx 20\,^{\circ}\mathrm{C\,min^{-1}}$ to 22 °C. When the moduli presented a plateau, indicating the reformation of the gel, strain sweep and frequency sweep were performed again to compare the results with the previous ones.

Self-healing properties of gel phases were also tested by rheometer; they were carried out at room temperature and at a frequency of 1 Hz, varying the strain from low to high percentage values for fixed time intervals of 5 minutes (values of yield strain to apply were chosen from linear viscoelastic region and destructive strain of the gel). Rotational strain was kept at 0% for 0.05 s before changing from destructive strain to linear viscoelastic region conditions. When the moduli reached plateau values after the cessation of disruptive strain, it was possible to calculate the percentage of recovery of the initial G' value. In those cases where the G' values oscillated or increased continuously, G' and G'' were measured at a fix strain and frequency for longer periods.

RLS measurements: RLS measurements were carried out with a spectrofluorophotometer using a synchronous scanning mode in which the emission and excitation monochromators were preset to identical wavelengths. The RLS spectrum was recorded from 300 to 600 nm with both the excitation and emission slit widths set at 1.5 nm. We chose as working wavelength the one corresponding to the intensity maximum of the emission spectrum. Samples for a typical kinetic measurement were prepared by injecting into a quartz cuvette (light path 0.2 cm) the limpid hot solution of salt. The measurements were carried out at 25 °C. Spectra were recorded until gel formation. The gel phase obtained at the end of the measurement was stable after the tube inversion test.

Opacity measurements: Opacity measurements were recorded with a spectrophotometer. The opacity of the gel phases was determined with UV/Vis measurements as a function of time, at a wavelength of 568 nm and a temperature of 25 °C. As described for RLS measurements, samples for a typical measurement were prepared by injecting into a quartz cuvette (light path 0.2 cm) a hot solution of salt. Spectra were recorded until gel formation. The gel phase obtained at the end of the measurement was stable according to the tube inversion test.

Thixotropic and sonotropic behavior: The gel phases obtained were subjected to two different external stimuli. The mechanical stimulus involved stirring the gel phase at 1000 rpm for 5 min, using a stirring bar (length 8 mm, height 3 mm). The sonotropic behavior of the gel phases was tested by irradiating in an ultrasound water bath for 5 min with a power of 200 W and a frequency of 45 kHz. Thereafter, the materials were stored at 4 °C overnight. When the samples were stable to the tube-inversion test, the gels were qualitatively defined as thixotropic or sonotropic.

Powder X-ray diffraction (XRD): Powder X-ray diffraction (XRD) patterns of samples were obtained on a Rigaku Ultima IV X-Ray diffractometer with $\mathrm{Cu_{K\alpha}}$ X-rays ($\lambda = 1.54$ Å) generated by a Rigaku generator operating at 40 kV and 30 mA with the collimator at 0.5 mm and a D/Tex detector.

Salts, solvents and gels were placed on a silicon substrate as thin films, and measurements were made overnight from 3 to 50 (°) in 2θ. The diffraction peaks for the gel networks were obtained by empirically subtracting the solvent components from the gel XRD patterns.[42a]

Acknowledgements

We thank MIUR (FIRB 2010RBFR10BF5V) and the US National Science Foundation (Grants CHE-1147353 and 1502856) for financial support. We thank Mr. Pasha Tabatabai of Georgetown University for help with the rheological measurements.

Keywords: gels · green chemistry · ionic liquids · organic salts · supramolecular gels

[1] a) P. Terech, R. G. Weiss, *Chem. Rev.* **1997**, *97*, 3133 – 3160; b) R. G. Weiss, P. Terech, *Molecular Gels, Materials with Self-Assembled Fibrillar Networks*, Springer, Dordrecht, **2006**.

[2] R. G. Weiss, *J. Am. Chem. Soc.* **2014**, *136*, 7519 – 7530.

[3] a) U. K. Das, V. G. Puranik, P. Dastidar, *Cryst. Growth Des.* **2012**, *12*, 5864 – 5868; b) V. A. Mallia, R. G. Weiss, *J. Phys. Org. Chem.* **2014**, *27*, 310 – 315.

[4] a) G. O. Lloyd, J. W. Steed, *Soft Matter* **2011**, *7*, 75 – 84; b) M. Rodrigues, A. C. Calpena, D. B. Amabilino, M. L. Garduno-Ramirez, L. Perez-Garcia, *J. Mater. Chem. B* **2014**, *2*, 5419 – 5429; c) P. Sahoo, N. N. Adarsh, G. E. Chacko, S. R. Raghavan, V. G. Puranik, P. Dastidar, *Langmuir* **2009**, *25*, 8742 – 8750; d) Y. Sun, X. Huang, *Supramol. Chem.* **2015**, *27*, 21 – 27.

[5] G. G. Eshetu, M. Armand, B. Scrosati, S. Passerini, *Angew. Chem. Int. Ed.* **2014**, *53*, 13342 – 13359; *Angew. Chem.* **2014**, *126*, 13558 – 13576.

[6] a) K. Hanabusa, H. Fukui, M. Suzuki, H. Shirai, *Langmuir* **2005**, *21*, 10383 – 10390; b) J. Le Bideau, L. Viau, A. Vioux, *Chem. Soc. Rev.* **2011**, *40*, 907 – 925.

[7] N. V. Plechkova, K. R. Seddon in *Methods and Reagents for Green Chemistry: An Introduction*, (Eds.: P. Tundo, A. Perosa, F. Zecchini), chap 5„ Wiley, New York, **2007**.

[8] D. Kim, G. Lee, D. Kim, J. S. Ha, *ACS Appl. Mater. Interfaces* **2015**, *7*, 4608 – 4615.

[9] N. Mohmeyer, D. Kuang, P. Wang, H.-W. Schmidt, S. M. Zakeeruddin, M. Gratzel, *J. Mater. Chem.* **2006**, *16*, 2978 – 2983.

[10] N. Kimizuka, T. Nakashima, *Langmuir* **2001**, *17*, 6759 – 6761.

[11] a) Z. Fan, Y. Wang, Z. Xue, L. Zhang, Y. Chen, S. Zhang, *J. Sol-Gel Sci. Technol.* **2014**, *72*, 328 – 333; b) Y. Ishioka, N. Minakuchi, M. Mizuhata, T. Maruyama, *Soft Matter* **2014**, *10*, 965 – 971; c) K. Rawat, J. Pathak, H. B. Bohidar, *Soft Matter* **2014**, *10*, 862 – 872; d) X. Zhu, H. Zhang, J. Wu, *Sens. Actuators B* **2014**, *202*, 105 – 113; e) M. Czugala, C. O'Connell, C. Blin, P. Fischer, K. J. Fraser, F. Benito-Lopez, D. Diamond, *Sens. Actuators B* **2014**, *194*, 105 – 113; f) T. M. Benedetti, T. Carvalho, D. C. Iwakura, F. Braga, B. R. Vieira, P. Vidinha, J. Gruber, R. M. Torresi, *Sol. Energy Mater. Sol. Cells* **2015**, *132*, 101 – 106.

[12] P. C. Marr, A. C. Marr, *Green Chem.* **2016**, *18*, 105 – 128.

[13] W. Jiang, J. Hao, Z. Wu, *Langmuir* **2008**, *24*, 3150 – 3156.

[14] M. Cai, Y. Liang, F. Zhou, W. Liu, *J. Mater. Chem.* **2011**, *21*, 13399 – 13405.

[15] W. Zhang, C. Yuan, J. Guo, L. Qiu, F. Yan, *ACS Appl. Mater. Interfaces* **2014**, *6*, 8723 – 8728.

[16] F. D'Anna, R. Noto, *Eur. J. Org. Chem.* **2014**, 4201 – 4223.

[17] F. D'Anna, C. Rizzo, P. Vitale, G. Lazzara, R. Noto, *Soft Matter* **2014**, *10*, 9281 – 9292.

[18] F. D'Anna, P. Vitale, F. Ferrante, S. Marullo, R. Noto, *ChemPlusChem* **2013**, *78*, 331 – 342.

[19] S. Raghavan, B. Cipriano in *Gel Formation: Phase Diagrams Using Tabletop Rheology and Calorimetry* (Eds.: R. Weiss, P. Terech), Springer, Dordrecht, **2006**, pp. 241 – 252.

[20] J. L. Anderson, R. Ding, A. Ellern, D. W. Armstrong, *J. Am. Chem. Soc.* **2005**, *127*, 593 – 604.

[21] F. D'Anna, H. Q. N. Gunaratne, G. Lazzara, R. Noto, C. Rizzo, K. R. Seddon, *Org. Biomol. Chem.* **2013**, *11*, 5836 – 5846.

[22] M. H. Nielsen, S. Aloni, J. J. De Yoreo, *Science* **2014**, *345*, 1158 – 1162.

[23] F. D'Anna, F. Ferrante, R. Noto, *Chem. Eur. J.* **2009**, *15*, 13059 – 13068.

[24] J. Kagimoto, N. Nakamura, T. Kato, H. Ohno, *Chem. Commun.* **2009**, 2405 – 2407.

[25] L. Crowhurst, P. R. Mawdsley, J. M. Perez-Arlandis, P. A. Salter, T. Welton, *Phys. Chem. Chem. Phys.* **2003**, *5*, 2790 – 2794.
[26] a) C. Daniel, C. Dammer, J.-M. Guenet, *Polymer* **1994**, *35*, 4243 – 4246; b) A. Garai, A. K. Nandi, *J. Polym. Sci. Part B* **2008**, *46*, 28 – 40.
[27] Z. Qi, N. L. Traulsen, P. M. de Molina, C. Schlaich, M. Gradzielski, C. A. Schalley, *Org. Biomol. Chem.* **2014**, *12*, 503 – 510.
[28] a) H. Bunzen, Nonappa, E. Kalenius, S. Hietala, E. Kolehmainen, *Chem. Eur. J.* **2013**, *19*, 12978 – 12981; b) H. Xu, J. Song, T. Tian, R. Feng, *Soft Matter* **2012**, *8*, 3478 – 3486.
[29] A. J. McLean, M. J. Muldoon, C. M. Gordon, I. R. Dunkin, *Chem. Commun.* **2002**, 1880 – 1881.
[30] a) X. Huang, S. R. Raghavan, P. Terech, R. G. Weiss, *J. Am. Chem. Soc.* **2006**, *128*, 15341 – 15352; b) Y. Ohsedo, M. Miyamoto, A. Tanaka, H. Watanabe, *New J. Chem.* **2013**, *37*, 2874 – 2880.
[31] a) M. Lescanne, P. Grondin, A. O'Aléo, F. Fages, J. L. Pozzo, O. M. Monval, P. Reinheimer, A. Colin, *Langmuir* **2004**, *20*, 3032 – 3041; b) V. A. Mallia, M. George, D. L. Blair, R. G. Weiss, *Langmuir* **2009**, *25*, 8615 – 8625.
[32] Y. Fang, J. Zhang, X. Zhou, Y. Lin, S. Fang, *Electrochim. Acta* **2012**, *68*, 235 – 239.
[33] P. Vitale, F. D'Anna, S. Marullo, R. Noto, *Soft Matter* **2015**, *11*, 6652 – 6662.
[34] B. Roy, P. Bairi, A. Saha, A. K. Nandi, *Soft Matter* **2011**, *7*, 8067 – 8076.
[35] X. Y. Liu, P. D. Sawant, *Appl. Phys. Lett.* **2001**, *79*, 3518 – 3520.
[36] X. Huang, P. Terech, S. R. Raghavan, R. G. Weiss, *J. Am. Chem. Soc.* **2005**, *127*, 4336 – 4344.
[37] a) R. F. Pasternack, C. Bustamante, P. J. Collings, A. Giannetto, E. J. Gibbs, *J. Am. Chem. Soc.* **1993**, *115*, 5393 – 5399; b) R. F. Pasternack, P. J. Collings, *Science* **1995**, *269*, 935 – 939.
[38] J. Anglister, I. Z. Steinberg, *J. Chem. Phys.* **1983**, *78*, 5358 – 5368.
[39] a) Y. Feng, Z.-X. Liu, H. Chen, Z.-C. Yan, Y.-M. He, C.-Y. Liu, Q.-H. Fan, *Chem. Eur. J.* **2014**, *20*, 7069 – 7082; b) L. Yu, Y. Zhang, R. Chen, D. Zhang, X. Wei, F. Chen, J. Wang, M. Xu, *Talanta* **2015**, *131*, 475 – 479.
[40] C. Rizzo, F. D'Anna, S. Marullo, P. Vitale, R. Noto, *Eur. J. Org. Chem.* **2014**, 1013 – 1024.
[41] a) M. Tena-Solsona, B. Escuder, J. F. Miravet, V. Casttelleto, I. W. Hamley, A. Dehsorkhi, *Chem. Mater.* **2015**, *27*, 3358 – 3365; b) P. Terech, D. Pasquier, V. Bordas, C. Rossat, *Langmuir* **2000**, *16*, 4485 – 4494.
[42] a) E. Ostuni, P. Kamaras, R. G. Weiss, *Angew. Chem. Int. Ed. Engl.* **1996**, *35*, 1324 – 1326; *Angew. Chem.* **1996**, *108*, 1423 – 1425; b) M. Zhang, S. Selvakumar, X. Zhang, M. P. Sibi, R. G. Weiss, *Chem. Eur. J.* **2015**, *21*, 8530 – 8543.
[43] S. Roy, A. Baral, A. Banerjee, *Chem. Eur. J.* **2013**, *19*, 14950 – 14957.
[44] a) A. Ajayaghosh, V. K. Praveen, *Acc. Chem. Res.* **2007**, *40*, 644 – 656; b) S. J. George, A. Ajayaghosh, *Chem. Eur. J.* **2005**, *11*, 3217 – 3227.
[45] F. D'Anna, S. La Marca, P. Lo Meo, R. Noto, *Chem. Eur. J.* **2009**, *15*, 7896 – 7902.

Received: February 12, 2016